Pergamon

Neural Networks, Vol. 10, No. 9, pp. 1673–1690, 1997

Printed in Great Britain
0893–6080/97 $17.00+.00

PII: S0893-6080(97)00023-3

CONTRIBUTED ARTICLE

Global Bifurcation Structure of Chaotic Neural Networks and its Application to Traveling Salesman Problems

ISAO TOKUDA,[1] TOMOMASA NAGASHIMA[1] AND KAZUYUKI AIHARA[2]

[1]Department of Computer Science and Systems Engineering, Muroran Institute of Technology and [2]Faculty of Engineering, The University of Tokyo

(*Received* 10 *May* 1996; *accepted* 30 *January* 1997)

Abstract—*This paper studies global bifurcation structure of the chaotic neural networks applied to solve the traveling salesman problem (TSP). The bifurcation analysis clarifies the dynamical basis of the chaotic neuro-dynamics which itinerates a variety of network states associated with possible solutions of TSP and efficiently 'searches' for the optimum or near-optimum solutions. By following the detailed merging process of chaotic attractors via crises, we find that the crisis-induced intermittent switches among the ruins of the previous localized chaotic attractors underly the 'chaotic search' for TSP solutions. On the basis of the present study, efficiency of the 'chaotic search' to optimization problems is discussed and a guideline is provided for tuning the bifurcation parameter value which gives rise to efficient 'chaotic search'.* © *1997 Elsevier Science Ltd. All rights reserved.*

Keywords—Chaotic neural network, Traveling salesman problem, Chaos, Bifurcation, Chaotic search, Chaotic itinerancy, Symmetry-increasing bifurcation.

1. INTRODUCTION

The traveling salesman problem (TSP) is a classic and famous example of a combinatorial optimization problem which is hard to deal with. Computational time required to find an exactly optimum solution grows faster than any finite power of some appropriate measure of the problem size as long as $P \neq NP$ (see e.g., Garey & Johnson, 1979; Lawler, Lenstra, Rinnooy Kan, & Shmoys, 1985; Reeves, 1993). In order to cope with such difficult problems, efficient approximate algorithms for finding a near-optimum solution within a reasonable computational time have been searched for. As one of such methods, this paper focuses on an intriguing optimization technique of TSP by chaotic dynamics (Nozawa, 1992, 1994; Yamada, Aihara & Kotani, 1993; Yamada & Aihara, 1994; Chen & Aihara, 1995) based on chaotic neural networks (Aihara, Takabe, & Toyoola, 1990).

In the neural network approach to TSP, every possible solution of the TSP is mapped into a network of neurons with (0,1)-binary outputs (Hopfield & Tank, 1985). Optimization by chaotic dynamics searches for a better TSP solution by following a chaotic wandering orbit. By visiting a variety of network states which correspond to possible solutions of the TSP, chaotic dynamics continually keeps searching for a better solution.

The chaotic dynamics in neural network models has been discussed in the earlier studies in the light of its potential biological functional role (Skarda & Freeman, 1987; Tsuda, Koerner, & Shimizu, 1987; Yao & Freeman, 1987; Aihara et al., 1990; Aihara, 1990; Tsuda, 1991b, 1992; Adachi & Aihara, 1996; Nagashima, Shiroki, & Tokuda, 1996). Freeman et al. suggested a functional role of chaos as a novelty filter when a rabbit memorizes a new odor (Skarda & Freeman, 1987; Yao & Freeman, 1987). Several researchers (Tsuda et al. 1987; Tsuda, 1992; Aihara, 1990; Adachi & Aihara 1996; Nagashima et al. 1996) observed chaotic neuro-dynamics which successively retrieves memory states stored with a Hebbian or auto-associative matrix of synaptic connections. Such dynamical process can be understood as the 'memory search' mechanism by

Acknowledgements: The authors wish to thank Professor T. Matsumoto (Waseda University), Professor I. Tsuda (Hokkaido University), Professor H. Kokubu (Kyoto University), and Professor R. Tokunaga (Tsukuba University) for stimulating discussions and continual encouragement on this work. They would also like to thank Professor M. Kubo (Tokyo University of Mercantile Marine) for his generous guidance to modern TSP studies and Professor K. Ikeda (Ritsumeikan University) for valuable comments on the original manuscript. They are also grateful to the reviewers of *Neural Networks* for careful reading of the manuscript, precious comments on the present study from the viewpoint of chaotic itinerancy, and constructive suggestions on our experiments.

Requests for reprints should be sent to: Isao Tokuda, Department of Computer Science and Systems Engineering, Muroran Institute of Technology, Muroran, Hokkaido 050, Japan. Tel: +81-143-47-3281; Fax: +81-143-47-3374; E-mail: tokuda@oyna.cc.muroran-it.ac.jp.

chaotic dynamics. Following the idea of the 'chaotic search' of memories, we call the chaotic dynamics which seeks a better TSP solution by a successive retrieval of a variety of TSP solutions 'chaotic search' for TSP solutions.

The remarkable 'chaotic search' capability to TSP is demonstrated by Nozawa (1992) who reported that for 94% of the random choices of initial conditions a chaotic neural network with heuristically tuned values of system parameters finds optimum solutions of a 10-city TSP within 1000-iterative steps. Whereas the experimental studies demonstrate efficiency of the 'chaotic search' to the optimization problem, we remark that they provide only preliminary results. Due to the complex dynamics of the chaotic neural network, the underlying dynamical mechanism of the 'chaotic search' is not at all clear. Hence, the efficiency of the method cannot be grasped theoretically.

The aim of the present paper is to clarify the underlying mechanism of the 'chaotic search' and to re-examine the efficiency of the method to optimization problems. The optimization mechanism is worthwhile investigating not only for engineering applications but also for understanding possible information processing carried out by chaotic dynamics in neural network models. For our aim, we study global bifurcation structure of the chaotic neural networks applied to solve TSPs. The bifurcation study not only clarifies the dynamical mechanism of the 'chaotic search' but also provides a guideline for tuning the bifurcation parameter value which gives rise to the network dynamics with efficient 'chaotic search'. While the guideline applies only to the bifurcation parameter, it may still reduce the amount of labor for adjusting many parameter values of the chaotic neural network by conventional trial and error methods.

The present paper is organized as follows: In Section 2, we review an experimental method for solving TSP by chaotic neural networks. In Sections 3 and 4, we study one-parameter bifurcation structure of the chaotic neural networks applied to 10- and 5-city instances of TSP. In particular, we follow in detail the merging process of chaotic attractors via crises (Grebogi, Ott, & York, 1982) and find that the crisis-induced intermittent switching (Grebogi, Ott, Romeiras, & York, 1987) underlies the 'chaotic search' for TSP solutions. In Section 5, on the basis of the bifurcation studies of Sections 3 and 4, we discuss the global bifurcation structure of the chaotic neural network and the practical applicability of the 'chaotic search' to the optimization problem. Since our bifurcation studies deal with chaotic neural networks applied to a limited number of TSP instances with an extremely small number of cities, our discussions cannot be straightforwardly applied to a general class of TSPs. We believe, however, that the present study describes the essential features of the bifurcation structure of the chaotic neural network and provides qualitative understanding of the 'chaotic search' mechanism which may efficiently work for a wide class of TSPs.

2. EXPERIMENT ON SOLVING TSP BY CHAOTIC NEURAL NETWORK

This section reviews the experimental method for solving TSP by chaotic neural networks (Nozawa, 1992). First, the Hopfield–Tank neural network is introduced to solve TSP. Second, chaotic neural network is derived by the Euler's discretization of the continuous-time Hopfield–Tank neural network. Third, a technique for observing a set of temporal firing rates of neurons as a possible TSP solution is described.

2.1. Hopfield–Tank Approach to TSP

Consider an N-city traveling salesman problem (TSP): Given an $N \times N$ symmetric matrix (d_{ij}) of distances between a set of N cities $(i,j = 0,1,\ldots,N-1)$, find a minimum-length tour that visits each city exactly once.

A solution for the TSP can be described in terms of a $N \times N$ matrix V with (0,1)-binary elements $\{V_{ik} = 0,1 \mid i,k = 0,1,\ldots,N-1\}$. Any complete tour can be represented by denoting $V_{ik} = 1$ if city i is in position k in the tour and $V_{ik} = 0$ otherwise. The position k stands for a visiting order in the tour (see Figure 1). Preference for the matrix V as a solution to the TSP can be measured by the following cost function:

$$E(V) = \frac{A}{2}\sum_{i=0}^{N-1}\{\sum_{k=0}^{N-1} V_{ik} - 1\}^2 + \frac{A}{2}\sum_{k=0}^{N-1}\{\sum_{i=0}^{N-1} V_{ik} - 1\}^2 + \frac{B}{2}\sum_{i=0}^{N-1}\sum_{j=0}^{N-1}\sum_{k=0}^{N-1} d_{ij} V_{ik}\{V_{j\,k+1} + V_{j\,k-1}\} \tag{1}$$

Whereas the first two terms represent the constraint terms to satisfy the feasibility condition of TSP and provide penalties for infeasible solutions for TSP, the third term represents a total path length of a complete tour of feasible TSP solutions. The solution matrix V associated with a low cost value represents a candidate of a good TSP solution, since the low cost solution may satisfy the constraints and provide a short length tour.

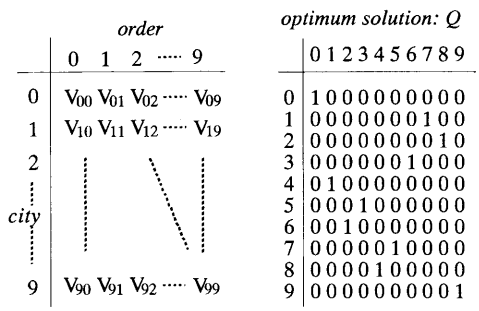

FIGURE 1. $N \times N$-element binary code $V = \{V_{ik} \mid i,k = 0,1,\ldots,N-1\}$ as a solution to TSP. Shown right is the optimum solution Q of the 10-city TSP studied in this paper. The solution represents a tour in which city 0 is the first city to be visited, city 4 the second, city 6 the third, and so forth.

On the basis of the representation of a TSP solution by the $N \times N$ matrix V, the Hopfield–Tank neural network (Hopfield & Tank, 1985) is designed as

$$R\left(\frac{d}{dt}u_{ik}\right) = -u_{ik} + \sum_{j=0}^{N-1}\sum_{l=0}^{N-1} T_{ik,jl}V_{jl} + I_{ik}, \quad V_{ik} = \sigma(u_{ik}) \tag{2}$$

where $0 \leq i,k \leq N-1$, u_{ik} stands for the internal state variable of the (i,k)-neuron, R stands for the time constant parameter, and $\sigma(x) = 0.5 + 0.5\tanh(x/\beta)$. The synaptic connections $T_{ik,jl}$ are given by

$$T_{ik,jl} = -A(\delta_{ij}(1-\delta_{kl}) + \delta_{kl}(1-\delta_{ij})) - Bd_{ij}(\delta_{l;k+1} + \delta_{l;k-1}), \ (i,k) \neq (j,l), \tag{3}$$

$$T_{ik,ik} = -2A, \tag{4}$$

$$I_{ik} = 2A, \tag{5}$$

for $0 \leq i,k,j,l \leq N-1$.

The Hopfield–Tank neural network (eqn (2)) has potential capability to solve the TSP because:

1. The underlying Lyapunov function is defined as $H(V) = E(V) + \sum_{i=0}^{N-1}\sum_{k=0}^{N-1}\int_0^{V_{ik}}\sigma^{-1}(V)\mathrm{d}V$ which is, for small β, nearly equal to the cost function of the TSP (eqn (1)), since $\sum_{i=0}^{N-1}\sum_{k=0}^{N-1}\int_0^{V_{ik}}\sigma^{-1}(V)\mathrm{d}V \rightarrow 0 (\beta \rightarrow 0)$.
2. Since, for small β, the minimal states of the Lyapunov function appear nearly with (0,1)-binary outputs $\{V_{ik} = 0, 1 \mid i,k = 0, 1, \ldots, N-1\}$, final equilibrium states of eqn (2) may provide feasible TSP solutions with short total-path length.

2.2. Experiment on Solving TSP by Chaotic Neural Network

Nevertheless, practical applicability of the Hopfield–Tank neural network to optimization problems is crucially limited by the following problems:

1. Choosing the parameter values for (A,B) which controls the strength of the constraint terms against the tour-length term in eqn (1) is quite difficult. In fact, it is reported in (Willson & Pawley, 1988; Hegde, Sweet, & Levy, 1988) that appropriate parameter values for (A,B) which properly locate feasible TSP solutions into local minima of the Lyapunov function $H(V)$ lie in a small restricted space. Most choices of (A,B) fail to locate feasible TSP solutions as the local minima and instead produce a large number of local minima which do not satisfy the constraints of eqn (1).
2. Even with an appropriate selection of the parameter values (A,B), the Lyapunov function $H(V)$ still has a large number of feasible solutions from long-length tours to nearly shortest tours. Due to the existence of the large number of long length tours which are far from the optimum tour, the network is frequently trapped in local minima with such bad solutions, depending on the choice of initial conditions.

For (1), various techniques are investigated for determining good parameter values for (A,B) (Willson & Pawley, 1988; Aiyer, Niranjan, & Frank, 1990; Ohta, Anzai, Yoneda, & Ogihara, 1993). For (2), stochastic dynamics is usually introduced to escape from the local minima with long length tours (Kirkpatrick, Gelatt, & Vecchi, 1983). In the chaotic neural network approach to TSP, the network escapes from the local minima by chaotic non-equilibrium dynamics (Aihara et al., 1990). The chaotic neural network for the combinatorial optimization problem is formulated as follows.

First, parameter values for the synaptic connections (eqns (3)–(5)) are slightly modified as

$$T_{ik,jl} = -A(\delta_{ij}(1-\delta_{kl}) + \delta_{kl}(1-\delta_{ij})) - Bd_{ij}(\delta_{l\,k+1} + \delta_{l\,k-1}), \ (i,k) \neq (j,l) \tag{6}$$

$$T_{ik,ik} = -2\omega A, \tag{7}$$

$$I_{ik} = 2\alpha A, \tag{8}$$

where $0 \leq i,k,j,l \leq N-1$, α is a control parameter for excitation level of neurons, and ω is a parameter for adjusting the negative self-feedback (Nozawa, 1992; Chen & Aihara, 1995) or the refractory effect (Aihara et al., 1990).

Second, with an affine transformation $u_{ik} = \sum_{j=0}^{N-1}\sum_{l=0}^{N-1} T_{ik,jl}\,p_{jl} + I_{ik}$, the Hopfield–Tank neural network (eqn (2)) is transformed into the following form

$$R\left(\frac{d}{dt}p_{ik}\right) = -p_{ik} + V_{ik},$$

$$V_{ik} = \sigma\left(\sum_{j=0}^{N-1}\sum_{l=0}^{N-1} T_{ik,jl}p_{jl} + I_{ik}\right). \tag{9}$$

If the connection matrix T is invertible, it is proved by Pineda (Pineda, 1988) that the attractor structure of the two equations (2) and (9) is identical. The chaotic neural network is then derived by the Euler's discretization of the continuous-time model (eqn (9)) as

$$p_{ik}(n+1) = p_{ik}(n) + \frac{\delta t}{R}\left(-p_{ik}(n) + \sigma\left(\sum_{j=0}^{N-1}\sum_{l=0}^{N-1} T_{ik,jl}p_{jl}(n) + I_{ik}\right)\right)$$

$$= rp_{ik}(n) + (1-r)\sigma\left(\sum_{j=0}^{N-1}\sum_{l=0}^{N-1} T_{ik,jl}p_{jl}(n) + I_{ik}\right) \tag{10}$$

where Δt is the time step of the Euler's discretization and $r = 1 - (\Delta t/R)$. The model is equivalent to a single internal state version of the chaotic neural network (Aihara et al., 1990; Nozawa, 1992, 1994).

With a set of well selected values of the parameters $(A,$

B, ω, α, β), the chaotic neural network exhibits chaotic dynamics which 'searches' for TSP solutions. The search procedure for TSP solutions can be observed by calculating the temporal firing rates of neurons as follows.

At every time step n, first, we compute short-term averaged firing rates $\rho(n) = \{\rho_{ik}(n) = (1/\omega)\sum_{j=0}^{\omega-1} p_{ik}(n-j) | i, k = 0, 1, \ldots, N-1\}$ of neurons with an averaging duration ω. The temporal network firing state $\rho(n)$ is then encoded into an $N \times N$-element binary code $J(n) = \{J_{ik}(n) | i, k = 0, 1, \ldots, N-1\}$ as

$$J_{ik}(n) = 1[\rho_{ik}(n) - \rho^*(n)] \tag{11}$$

where $1[x] = 1$ $(x \geq 0)$, $1[x] = 0$ $(x < 0)$, and $\rho^*(n)$ is the N-th largest value among $\{\rho_{ik}(n) | i, k = 0, 1, \ldots, N-1\}$.

By wandering around a variety of $N \times N$-element binary codes $\{J(n) | n = 0,1,\ldots\}$ with possible TSP solutions, chaotic dynamics 'searches' for a better TSP solution. In particular, it is reported by Nozawa (1992) that, for 94% of the random choices of initial conditions, chaotic neural network with heuristically tuned values of the system parameters quickly searches for an optimum solution of a 10-city TSP. In the next section, we study the dynamical basis of such 'chaotic search'.

3. ONE-PARAMETER BIFURCATION OF THE CHAOTIC NEURAL NETWORK APPLIED TO SOLVE 10-CITY TSP

The experiment of applying the chaotic neural network to solve the Hopfield–Tank's 10-city TSP is carried out by Nozawa (1992, 1994) with a set of fixed parameter values. By taking one of the parameters as a bifurcation parameter, we study one-parameter bifurcation structure of the chaotic neural network and clarify the dynamical mechanism of the Nozawa experiment.

First, we show that the chaotic neural network (eqn (10)) has symmetry which characterizes the global bifurcation structure. Second, a simple coding rule which enables to map every attractor of the dynamical system to a possible TSP solution is introduced. Third, one-parameter bifurcation structure of the chaotic neural network is studied.

3.1. Symmetry in Dynamical Systems

Consider a set of transformations $G = \{\eta^l \circ \gamma^m | \, l = 0, 1, m = 0, \ldots, N-1, (l, m) \neq (0, 0)\}$ with $N \times N$-dimensional linear transformations of γ and η defined as

$$\gamma : p_{ik} \mapsto p_{i\,(k+1) \bmod N} \text{ for } 0 \leq i, k \leq N-1, \tag{12}$$

$$\eta : p_{ik} \mapsto p_{i\,(N-k) \bmod N} \text{ for } 0 \leq i, k \leq N-1, \tag{13}$$

where $\circ$ denotes composition.

By using an $N \times N$-dimensional mapping $f: R^{N \times N} \to R^{N \times N}$, let us denote the network dynamics of eqn (10) by $p(n+1) = f(p(n))$. Since $f \circ g = g \circ f$ for any $g \in G$ (see Appendix A), the dynamical system is invariant under the operation by any $g \in G$. Hence the set of transformations G provides symmetry of the dynamical system (eqn (10)).

The idea of the symmetry is important, because if $O = \{p(n) | \, n = 0,1,\ldots\}$ is any solution of the dynamical system, then so is $g(O) = \{g(p(n)) | \, n = 0,1,\ldots\}$ for all $g \in G$. In particular, if O is an attractor, then so is $g(O)$ for all $g \in G$. We then say that $g(O)$ is conjugate to O. With respect to the system symmetry, we can also characterize an attractor O by the following symmetry group (Golubitsky et al., 1988):

$$\Delta_O = \{g \in G | g(O) = O\}. \tag{14}$$

In the sense that the above group measures the degree of symmetry of O, we say that an attractor O is a Δ_O-symmetric attractor. If $\Delta_O = \emptyset$, we then say that an attractor O is an asymmetric attractor.

3.2. Coding of Attractors

In the study of high-dimensional dynamical systems which give rise to multi-stability of many attractors, introduction of a simple coding of attractors is useful for a systematic analysis of the system. For instance, in the study of globally coupled map (Kaneko, 1990, 1991), a large number of multi-stable attractors are coded by the clustering conditions, while, in the study of optical system (Ikeda & Matsumoto, 1987), attractors are coded by the branching order of the harmonic bifurcations. In the present analysis, every attractor in the neural dynamical system is coded into a possible TSP solution as follows.

First, a set of long-term average firing rates $\{\bar{\rho}_{ik} = \lim_{T \to \infty}(1/T)\sum_{n=0}^{T-1} p_{ik}(n) | i, k = 0, 1, \ldots, N-1\}$ is measured on an attractor $\{p(n) | n = 0,1,\ldots\}$. The attractor is then encoded into an $N \times N$-element binary code $\bar{J} = \{\bar{J}_{ik} | i, k = 0, 1, \ldots, N-1\}$ defined as

$$\bar{J}_{ik} = 1[\bar{\rho}_{ik} - \bar{\rho}^*] \tag{15}$$

where $\bar{\rho}^*$ is the N-th largest value among $\{\bar{\rho}_{ik} | i, k = 0, 1, \ldots, N-1\}$.

As is shown in Appendix B, a set of conjugate attractors $\{\eta^l \circ \gamma^m(O) | l = 0, 1, \; m = 0, \ldots, N-1\}$ are coded into an equivalent TSP solution by this coding, where $O = \{p(n) | n = 0,1,\ldots\}$ stands for an asymmetric attractor.

3.3. One-Parameter Bifurcation of the Chaotic Neural Network

Taking r as a bifurcation parameter, let us study one-parameter bifurcation structure of the chaotic neural network applied to solve the Hopfield–Tank's 10-city TSP, where the city locations are given in 2-dimensional coordinates as (0.2439, 0.1463), (0.8488, 0.3609), (0.6683, 0.2536), (0.6878, 0.5219), (0.1707, 0.2293), (0.2293, 0.7610), (0.4000, 0.4439), (0.8732, 0.6536), (0.5171, 0.9414), (0.6195, 0.2634) (Hopfield & Tank, 1985;

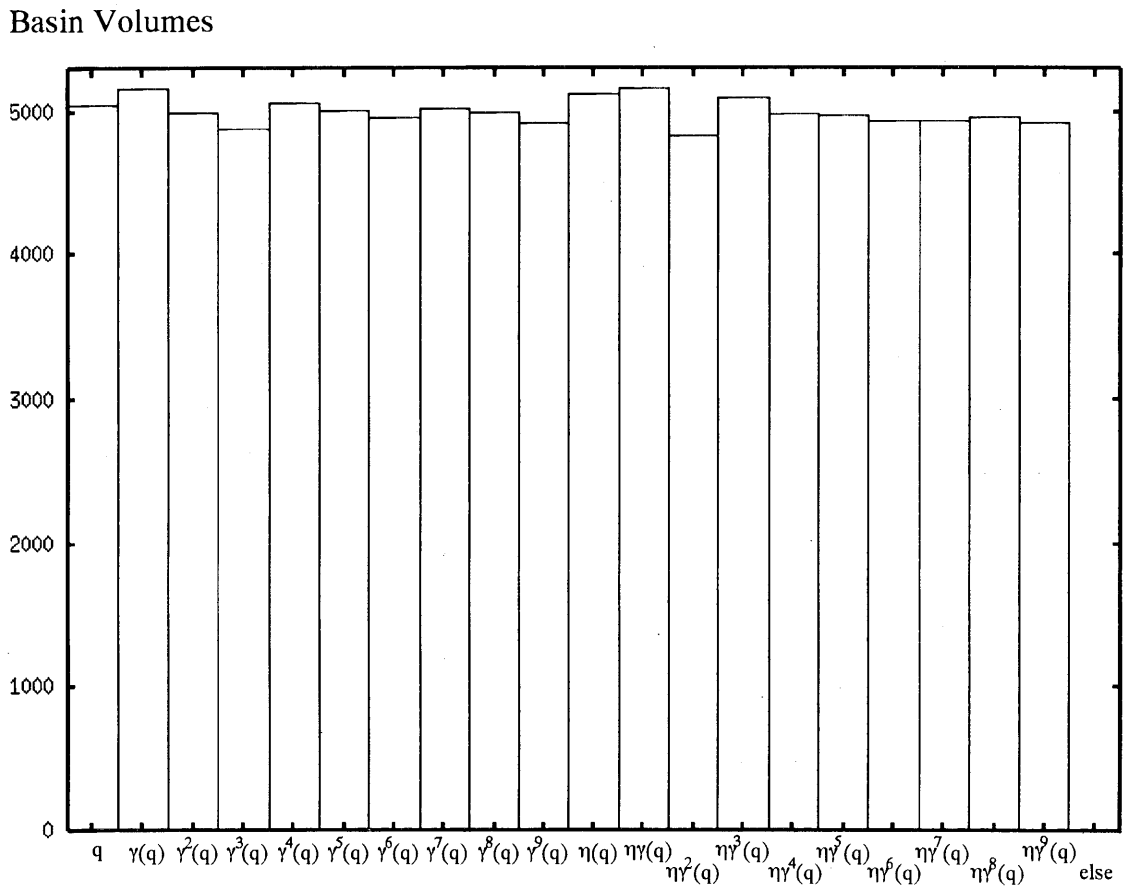

FIGURE 2. 100,000 samples of random initial conditions $p(0) \in [0,1]^{N\times N}$ are classified into basins of 20 conjugate fixed points $\{\eta^l \circ \gamma^m q | l = 0,1,\ m = 0,\ldots,9\}$ ($q(\in R^{N\times N}$) denotes a basic fixed point) or other attractors in the chaotic neural network with $r = 0.99$. The abscissa indicates the 20 conjugate fixed points and the other attractors, and the ordinate indicates the number of initial conditions included in the basin of each attractor.

Willson & Pawley, 1988). The values of the parameters are fixed as $(A, B, \omega, \alpha, \beta) = (1.0, 1.0, 0.75, 0.05, 0.018)$ so that the experimental situation of Nozawa (1992) is reproduced at $r = 0.70$.

As is discussed in Section 2, the chaotic neural network approaches to the continuous-time Hopfield–Tank neural network when $r \to 1.0$. Hence, parameter values close to $r = 1$ are expected to give rise to local minimum solutions of the Lyapunov function. First, by setting the parameter value to $r = 0.99$, we find the local minimum solutions by a carpet-bombing algorithm. From 100,000 samples of random initial conditions which are uniformly distributed over $p(0) \in [0,1]^{N\times N}$, only a set of $2N$ conjugate local minima $\{\eta^l \circ \gamma^m(q) | l = 0,1,\ m = 0,\ldots,N-1\}$ are found, where $q(\in \mathcal{R}^{N\times N})$ denotes a basic local minimum (see Figure 2).

By giving this q as the initial condition at $r = 0.89$ and decreasing the bifurcation parameter from $r = 0.89$ to $r = 0.65$, the bifurcation diagram is drawn by observing the (0,0)-neuron state $p_{00}(n)$ (see Figure 3(a) and (b)). The successively observed attractors are coded into possible TSP solutions $\bar{J}$ and the corresponding cost function values $E(\bar{J})$ defined by eqn (1) are plotted in Figure 3(c). We remark that until about $r \cong 0.725$ the cost function curve constantly holds the value corresponding to the optimum-tour length of the TSP. Namely, all the observed attractors until $r \cong 0.725$ are coded as the optimum solution. We denote this optimum solution code by Q (see Figure 1).

Figure 3(d) shows the Lyapunov dimension D_L (Kaplan & York, 1987) of the attractors observed in the bifurcation diagram.

(1) When $0.89 > r > 0.725$: In the first stage of this parameter region, the local minimum q continually exists until $r \cong 0.87$ and then undergoes a cascade of period-doubling bifurcations leading to a chaotic attractor (see Figure 3(b)). With a decrease in the bifurcation parameter, the chaotic attractor continually increases in size. Whereas the repeated occurrence of saddle-node bifurcations gives rise to pairs of stable and unstable periodic solutions generating periodic windows in the bifurcation diagram, the stable periodic attractors also bifurcate into chaotic attractors which merge with the original chaotic attractor via an interior crisis (Grebogi et al., 1982). Figure 4 illustrates how the unstable periodic orbits which are born from the period-doubling bifurcations of the local minimum q underlie the structure of the chaotic attractors.

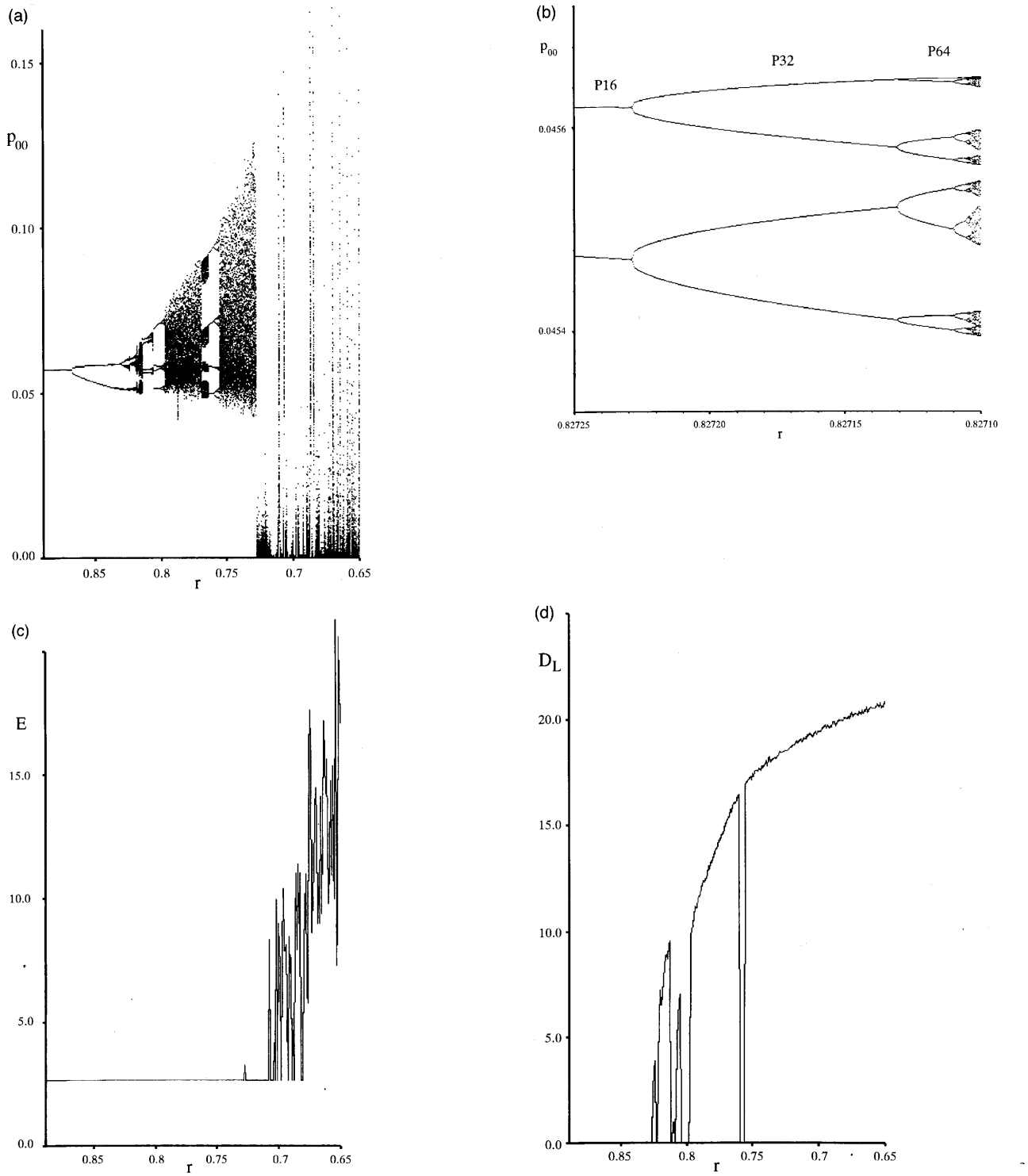

FIGURE 3. A one-parameter bifurcation diagram of the chaotic neural network for the 10-city TSP. The bifurcation parameter value r is decreased from 0.89 to 0.65. (a) A one-parameter bifurcation diagram observed from the (0,0)-neuron state $p_{00}(n)$. (b) Enlargement of the bifurcation diagram of (a). The period-16 attractor bifurcates into period-32, period-64, and so forth into a chaotic attractor. (c) The cost function values $E(\bar{J}(O_r))$ defined by eqn (1) for the successively observed attractors O_r in (a). The Lyapunov dimension D_L of the successively observed attractors O_r in (a).

Let us denote the successively observed attractors in Figure 3(a) by O_r, which depends upon the value of the bifurcation parameter r. Then the system symmetry implies that a conjugate attractor $\eta^l \circ \gamma^m(O_r)$ also undergoes a series of same bifurcations with O_r in this parameter region. Note that a conjugate attractor $\eta^l \circ \gamma^m(O_r)$ described above is continually coded as $\eta^l \circ \gamma^m(Q)$, which represents the optimum solution (see Appendix B).

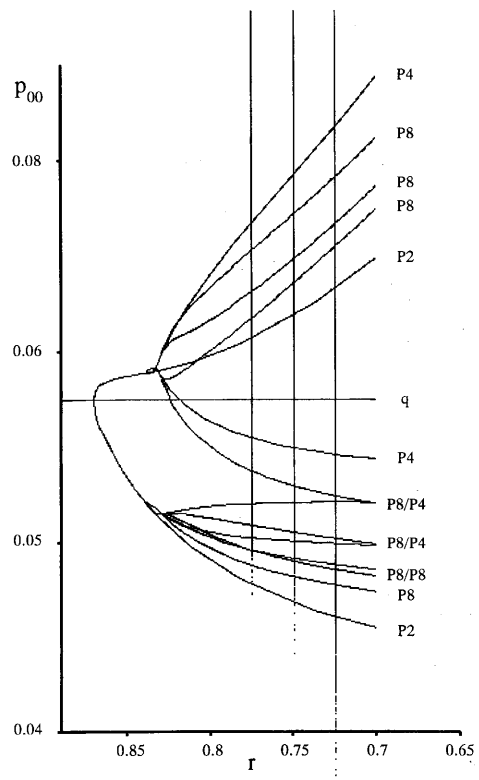

FIGURE 4. Period-2, 4, and 8 orbits born from the period-doubling bifurcations of the local minimum *q*. The figure displays how these unstable periodic orbits underly the structure of the chaotic attractors at $r = 0.775$, 0.750 and 0.725.

At most stages of their successive bifurcations, only the $2N$ conjugate attractors $\{\eta^l \circ \gamma^m(O_r) | l = 0,1, m = 0,\ldots,N-1\}$ are the observable attractors of the system. For instance, for systems with $r = 0.89$, 0.85, 0.78, 0.75, our numerical experiments show that all the initial conditions on a hyper-surface: $(p_{00},p_{01}) \in [0,1] \times [0,1], p_{02} = p_{03} = \cdots = p_{99} = 0$ can be classified into basins of the conjugate attractors $\{\eta^l \circ \gamma^m(O_r) | l = 0,1, m = 0,\ldots,N-1\}$ (see Figure 5(a)–(f)).

(2) When $0.74 > r$: As is shown in Figure 3(d), the $2N$ conjugate chaotic attractors increase their size as the bifurcation parameter is further decreased. When the parameter reaches a value of about $r \cong 0.725$, the thick chaotic band suddenly disappear from the bifurcation diagram of Figure 3(a). It seems that the $2N$ conjugate chaotic attractors collide with each other and merge as a single attractor via symmetry-increasing crises (Chossat & Golubitsky, 1988a, b).

3.4. Switching Among Previous Localized Chaotic Attractors and Chaotic Search for TSP Solutions

Let us study the network dynamics after the mergers of the $2N$ conjugate chaotic attractors via crises. The crises may give rise to intermittent switching among the previous localized chaotic attractors (Grebogi et al., 1987). By following the details of the switches, we find that the crisis-induced intermittent switches are the dynamical bases of the 'chaotic search' for TSP solutions.

Recalling that the basic attractors O_r observed in the bifurcation diagram in Figure 3(a) have been continually coded as the optimum solution Q, we denote the set of the conjugate chaotic attractors $\{\eta^l \circ \gamma^m(O_r) | l = 0,1, m = 0,\ldots,N-1\}$ just before the crises by $\{\eta^l \circ \gamma^m(Q) | l = 0,1, m = 0,\ldots,N-1\}$. Then, we can follow the details of the switches among the ruins of the previous localized chaotic attractors $\{\eta^l \circ \gamma^m(Q)\}$ by calculating the temporal network firing state $J(n)$ defined by eqn (11) with an averaging duration ω. For instance, if $J(n) = \eta^l \circ \gamma^m(Q)$, then we may consider that the temporal network firing state at the time step n is calculated over the duration during which the system is around the (l,m)-previous localized chaotic attractor $\eta^l \circ \gamma^m(Q)$.

Figure 6(a) shows a sequence $\{J(n) | n = 0,1,\ldots\}$ of the temporal network dynamics with $r = 0.73$. The dynamic behavior is from a given random initial condition and the averaging duration is set to $\omega = 500$. Starting from Q, cyclic switches among the previous localized chaotic attractors as

$$"Q \to \gamma(Q) \to \cdots \to \gamma^m(Q) \to \gamma^{m+1}(Q) \to \cdots \to \gamma^9(Q) \to Q" \tag{16}$$

are recognized. From a different initial condition, cyclic switches as

$$"\eta(Q) \to \eta\circ\gamma(Q) \to \cdots \to \eta\circ\gamma^m(Q) \to \eta\circ\gamma^{m+1}(Q) \to \cdots \to \eta\circ\gamma^9(Q) \to \eta(Q)" \tag{17}$$

are also observed. This implies that a first crisis gives birth to two attractors (16) and (17), which are conjugate with respect to η.

Figure 7 shows an average of the residence time τ_{av} (Grebogi et al., 1987), in which the network stays in one of the previous localized chaotic attractors $\{\eta^l \circ \gamma^m(Q) | l = 0,1, m = 0,\ldots,N-1\}$. At the initial stage of the crisis, switching rarely occurs and the residence time τ_{av} is inordinately long. As is explained in detail below, with a decrease in the bifurcation parameter, the previous localized chaotic attractors get more tightly connected to each other. This shortens the residence time τ_{av} in Figure 7.

For $0.73 \leq r \leq 0.737$, the system exhibits cyclic switching as (16) and (17). As the crisis proceeds for $0.66 < r < 0.73$, reversible switches such as

$$"Q \rightleftharpoons \gamma(Q) \rightleftharpoons \cdots \rightleftharpoons \gamma^m(Q) \rightleftharpoons \gamma^{m+1}(Q) \rightleftharpoons \cdots \rightleftharpoons \gamma^9(Q) \rightleftharpoons Q" \tag{18}$$

and

$$"\eta(Q) \rightleftharpoons \eta\circ\gamma(Q) \rightleftharpoons \cdots \rightleftharpoons \eta\circ\gamma^m(Q) \rightleftharpoons \eta\circ\gamma^{m+1}(Q) \rightleftharpoons \cdots \rightleftharpoons \eta\circ\gamma^9(Q) \rightleftharpoons \eta(Q)" \tag{19}$$

are observed (see Figure 6(b)). Irregular switches which

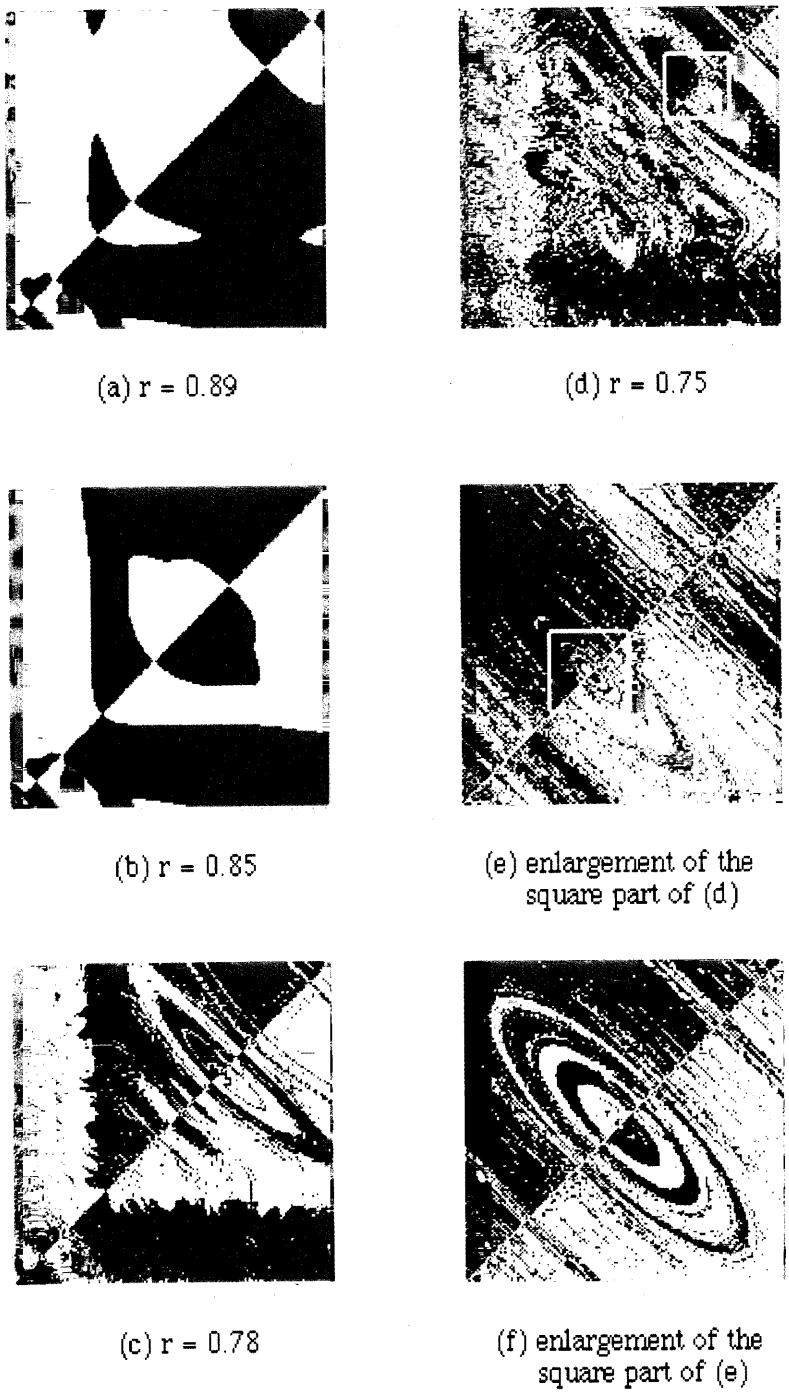

FIGURE 5. On the hyper-surface with $(p_{00},p_{01}) \in [0,1] \times [0,1]$, $p_{02} = p_{03} = \cdots = p_{99} = 0$, basin portraits of the conjugate attractors $\eta^l \circ \gamma^m(O_r) | l = 0,1$, $m = 0,\ldots,N-1$ are drawn for four systems: (a) $r = 0.89$, (b) $r = 0.85$, (c) $r = 0.78$, and (d) $r = 0.75$. The abscissa indicates $p_{00} \in [0,1]$ and the ordinate indicates $p_{01} \in [0,1]$. While (e) shows an enlargement of the square part: $(p_{00},p_{01}) \in [0.65,0.85] \times [0.65,0.85]$ of (d), (f) shows a further enlargement of the square part: $(p_{00},p_{01}) \in [0.707,0.757] \times [0.707,0.757]$ of (e). The basic attractors O_r are adopted from the ones observed in the bifurcation diagram of Figure 3(a). Basins of $\{\eta^l \circ \gamma^m(O_r) | l = 0,1, m = 0,\ldots,N-1\}$ are colored as follows: Basins of: $O_r, \gamma^7(O_r), \eta \circ \gamma^4(O_r)$ (yellow); $\gamma(O_r), \gamma^8(O_r), \eta \circ \gamma^5(O_r)$ (red); $\gamma^2(O_r), \gamma^9(O_r), \eta \circ \gamma^6(O_r)$ (green); $\gamma^3(O_r), \eta(O_r), \eta \circ \gamma^7(O_r)$ (black); $\gamma^4(O_r), \eta \circ \gamma(O_r), \eta \circ \gamma^8(O_r)$ (blue) $\gamma^5(O_r), \eta \circ \gamma^2(O_r), \eta \circ \gamma^9(O_r)$ (skyblue); $\gamma^6(O_r), \eta \circ \gamma^3(O_r)$ (purple).

skip the intermediate states as "$\gamma(Q) \rightleftharpoons \gamma^3(Q)$" or "$\eta \circ \gamma^5(Q) \rightleftharpoons \eta \circ \gamma^8(Q)$" are also observed for systems with small r.

For $r \leq 0.66$, the two conjugate attractors (18) and (19) finally merge into a fully-connected attractor via a second crisis. Chaotic dynamics which 'searches' for all the $2N$ previous localized chaotic attractors is observed in this region (see Figure 6(c)).

We remark that, by the first and the second crises, the originally asymmetric attractors $\{\eta^l \circ \gamma^m(O_r) | \ l = 0,1,$

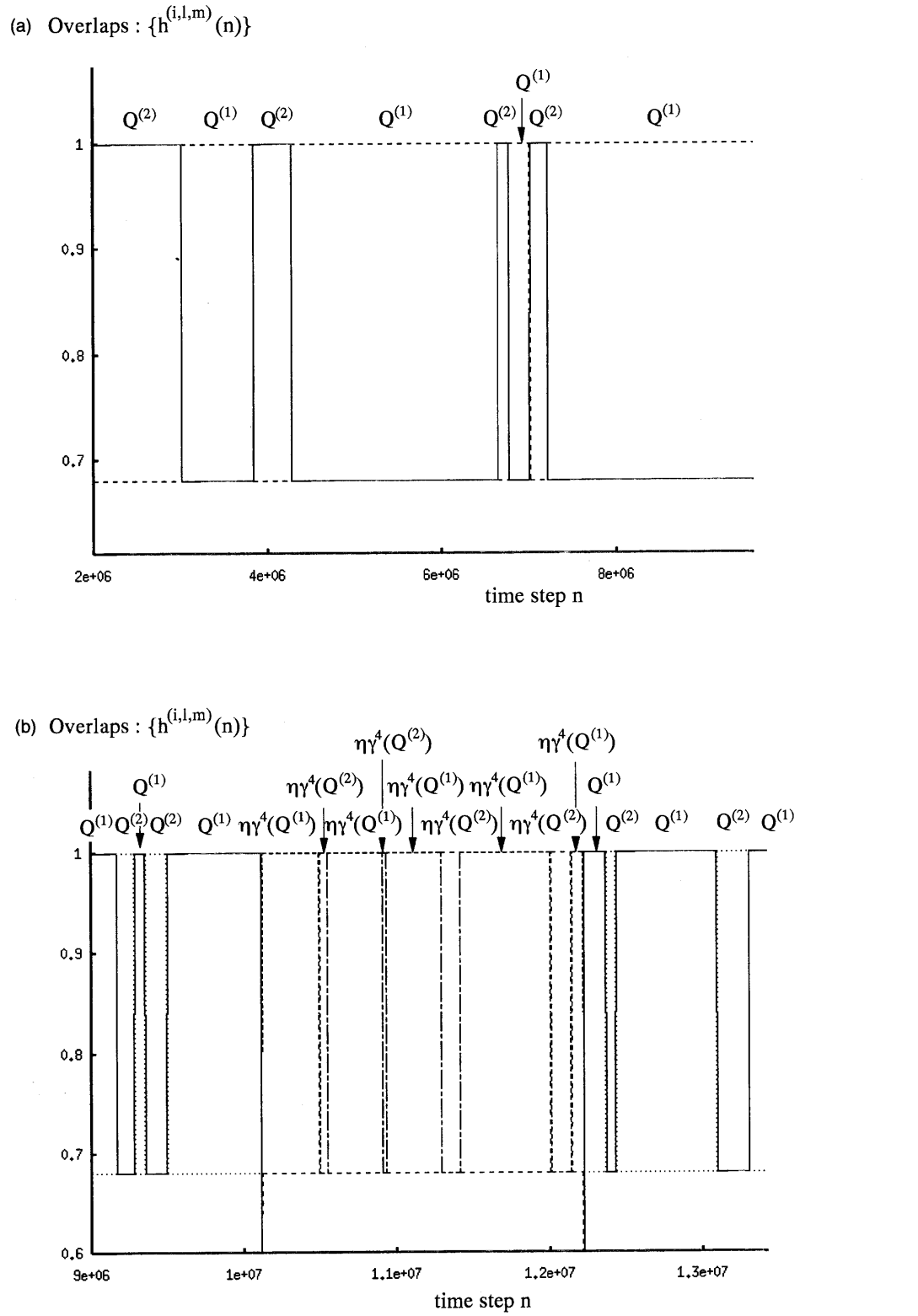

FIGURE 6. Sample sequences $\{J(n)|\ n = 0,1,\ldots\}$ of the temporal network dynamics with (a): $r = 0.730$, (b): $r = 0.702$, and (c): $r = 0.666$ are shown. The averaging duration of eqn (11) is set to $w = 500$. The temporal network state is displayed in terms of a set of overlaps between $J(n)$ and the previous localized chaotic attractors $\{\eta^l \circ \gamma^m(Q)|\ l = 0,1,\ m = 0,\ldots,9\}$, where the overlap between $J(n)$ and $\eta^l \circ \gamma^m(Q)$ is defined as

$$h^{(l,m)}(n) = \frac{1}{N^2} \sum_{i=0}^{N-1} \sum_{k=0}^{N-1} (2\{\eta^l \circ \gamma^m(Q)\}_{ik} - 1)(2J_{ik}(n) - 1).$$

(c) Overlaps : $\{h^{(l,m)}(n)\}$

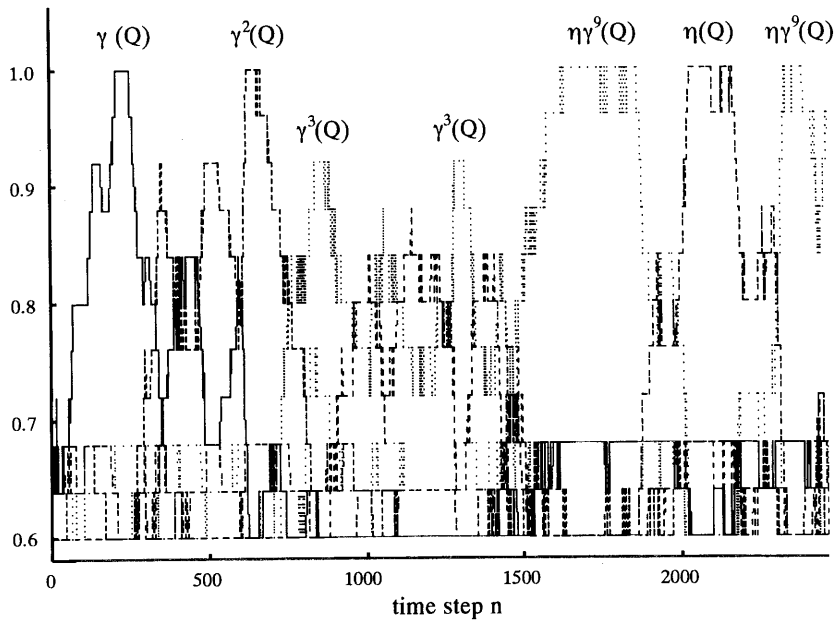

FIGURE 6. Continued.

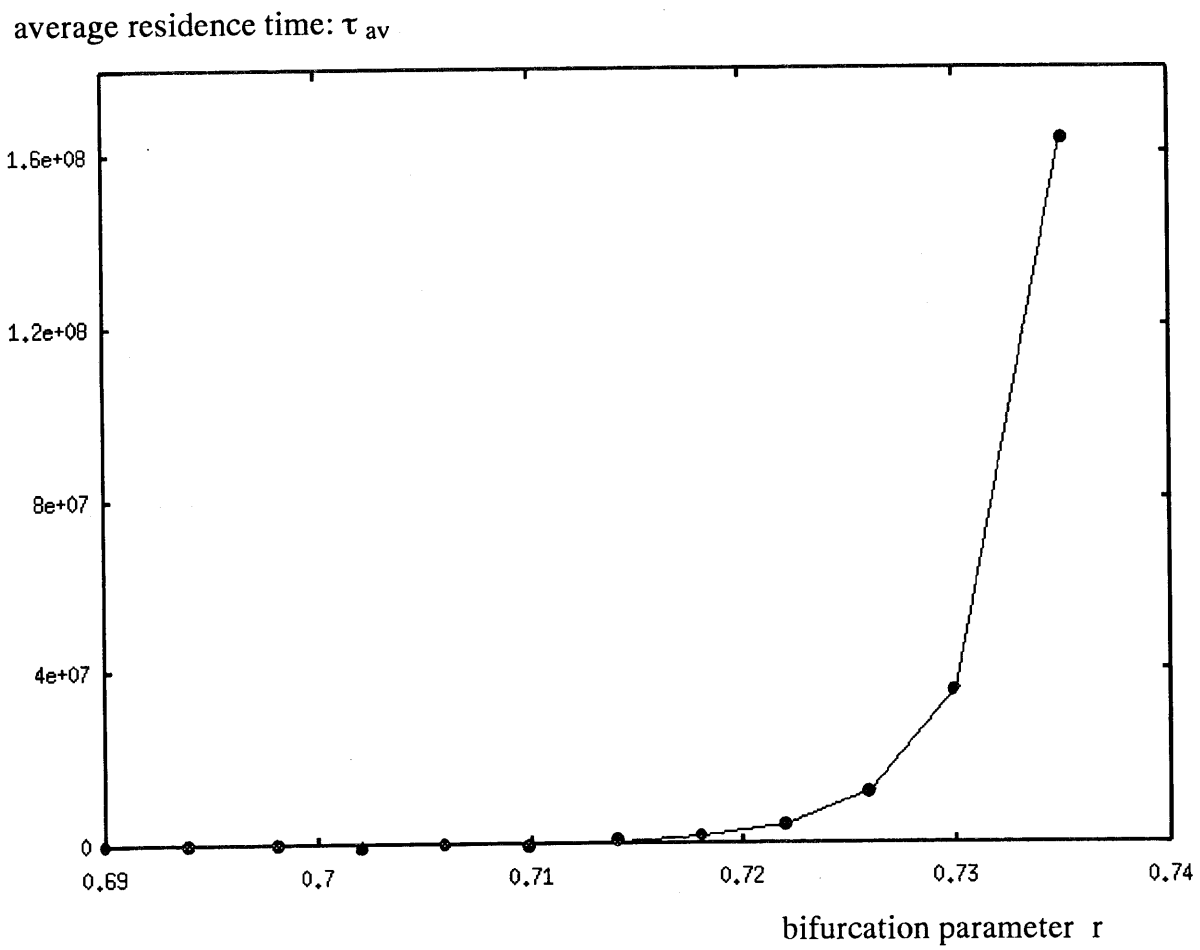

FIGURE 7. The average of residence time τ_{av} in a previous localized chaotic attractor $\{\eta^l \circ \gamma^m(Q) | \ l = 0,1, \ m = 0,\ldots,9\}$ is drawn with increasing the value of the bifurcation parameter *r*.

$m = 0,\ldots,N-1\}$ not only increase in size but also increase in symmetry from $\emptyset$-symmetry to G-symmetry. This is a symmetry-increasing bifurcation phenomenon of chaotic attractors which are commonly observed in dynamical systems with symmetry (Grebogi et al., 1987; Chossat & Golubitsky, 1988a, b).

3.5. Remarks on the Chaotic Itinerancy

In recent studies of high-dimensional dynamical systems, dynamical phenomena called as 'chaotic itinerancy' (Ikeda et al., 1989; Kaneko, 1990, 1991; Tsuda, 1991a, b, 1992) have been extensively studied. The chaotic itinerancy is characterized by high-dimensional chaotic behavior that makes intermittent transitions among a variety of 'attractor ruins' which are quasi-stationary sates with effectively low degrees of freedom. Chaotic itinerancy has been discovered in optical systems (Ikeda et al., 1989), coupled map models (Kaneko, 1990, 1991) and model neural networks (Tsuda, 1991a, b, 1992). As is initially suggested by Nozawa (1992, 1994), the present 'chaotic search' dynamics for optimization problems can also be considered as the chaotic itinerancy, although the dynamical mechanism such as the structure of the 'attractor ruins' has not been well described. Our bifurcation analysis clarifies the dynamical basis of the chaotic itinerancy in the 'chaotic search' dynamics in the context of the crisis-induced intermittent switching among the ruins of the previously stable chaotic attractors.

It should also be remarked that, in the study of globally coupled map, although no detailed analysis is presented, Kaneko (1990, 1991) suggested crisis-induced intermittency as the dynamical mechanism of the chaotic itinerancy. In the study of spatial pattern dynamics in locally coupled map, Kaneko (1989) also presented a bifurcation scenario for the onset of pattern competition intermittency via crisis, although the pattern competition intermittency is not directly related with the chaotic itinerancy. Our bifurcation analysis presents a practical example of a considerably simple bifurcation phenomenon for the onset of 'chaotic itinerancy' via crisis.

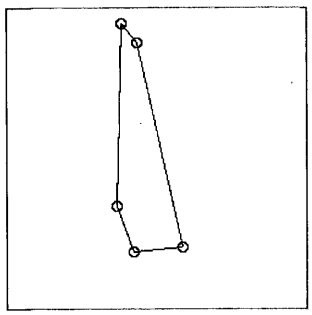

(a) Optimum tour: $Q^{(1)}$

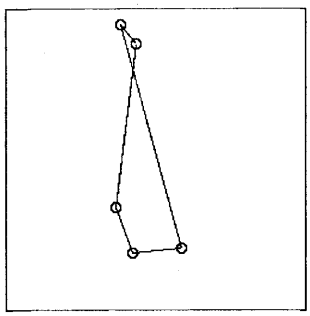

(b) Second-optimum tour: $Q^{(2)}$

FIGURE 8. Locations of the 5-cities, which are given in 2-dimensional coordinates as (0.3676, 0.3477), (0.4234, 0.1931), (0.5864, 0.2097), (0.3830, 0.9543), (0.4356, 0.8893): (a) represents an optimum tour $Q^{(1)}$ with a total path length of $d = 1.714747$; (b) represents a second-optimum tour $Q^{(2)}$ with a total path length of $d = 1.729555$.

4. APPLICATION TO 5-CITY TSP

In Section 3, we have seen that the crisis-induced switch is the dynamical basis of the 'chaotic search' in the 10-city TSP instance. Whereas the previous example shows 'chaotic search' among equivalent solutions to the TSP, by using a 5-city TSP instance, this section shows another example which exhibits 'chaotic search' among the optimum solution and the second-optimum solution to TSP.

4.1. One-Parameter Bifurcation of 5-City TSP

As an instance for TSP, 5-city locations were randomly generated (see Figure 8). The parameter values for the

TABLE 1

For 100,000 samples of random initial conditions which are uniformly distributed over $p(0) \in [0,1]^{5\times5}$, basin distribution rates to the two sets of conjugate attractors $\{\eta^l \circ \gamma^m(O_r^{(i)}) | \ i = 1,2, \ l = 0,1, \ m = 0,\ldots,4\}$ are calculated for systems with $r = 0.999$, $r = 0.900$, $r = 0.875$, $r = 0.850$ and $r = 0.825$. The basic attractors $O_r^{(1)}$ and $O_r^{(2)}$ are those observed in the bifurcation diagrams of Figure 9(a) and (c), respectively

Bifurcation parameter	Total basin volumes of $\{\eta^l \circ \gamma^m(O_r^{(1)}) \mid l = 0,1, \ m = 0,\ldots,4\}$	Total basin volumes of $\{\eta^l \circ \gamma^m(O_r^{(2)}) \mid l = 0,1, \ m = 0,\ldots,4\}$
$r = 0.999$	71.538 [%]	28.462 [%]
$r = 0.900$	72.966 [%]	27.034 [%]
$r = 0.875$	75.857 [%]	24.143 [%]
$r = 0.850$	75.304 [%]	24.696 [%]
$r = 0.825$	58.758 [%]	41.242 [%]

chaotic neural network are set to $(A, B, \omega, \alpha, \beta) = (1.5, 1.0, 0.80, 0.05, 0.018)$. The parameter values are slightly modified from the 10-city instance so that for $r \cong 1.0$ the continuous-time Hopfield–Tank neural network (eqn (9)) gives rise to feasible TSP solutions as the local minima.

First, for $r = 0.999$, we find the local minimum solutions of the continuous-time Hopfield–Tank neural

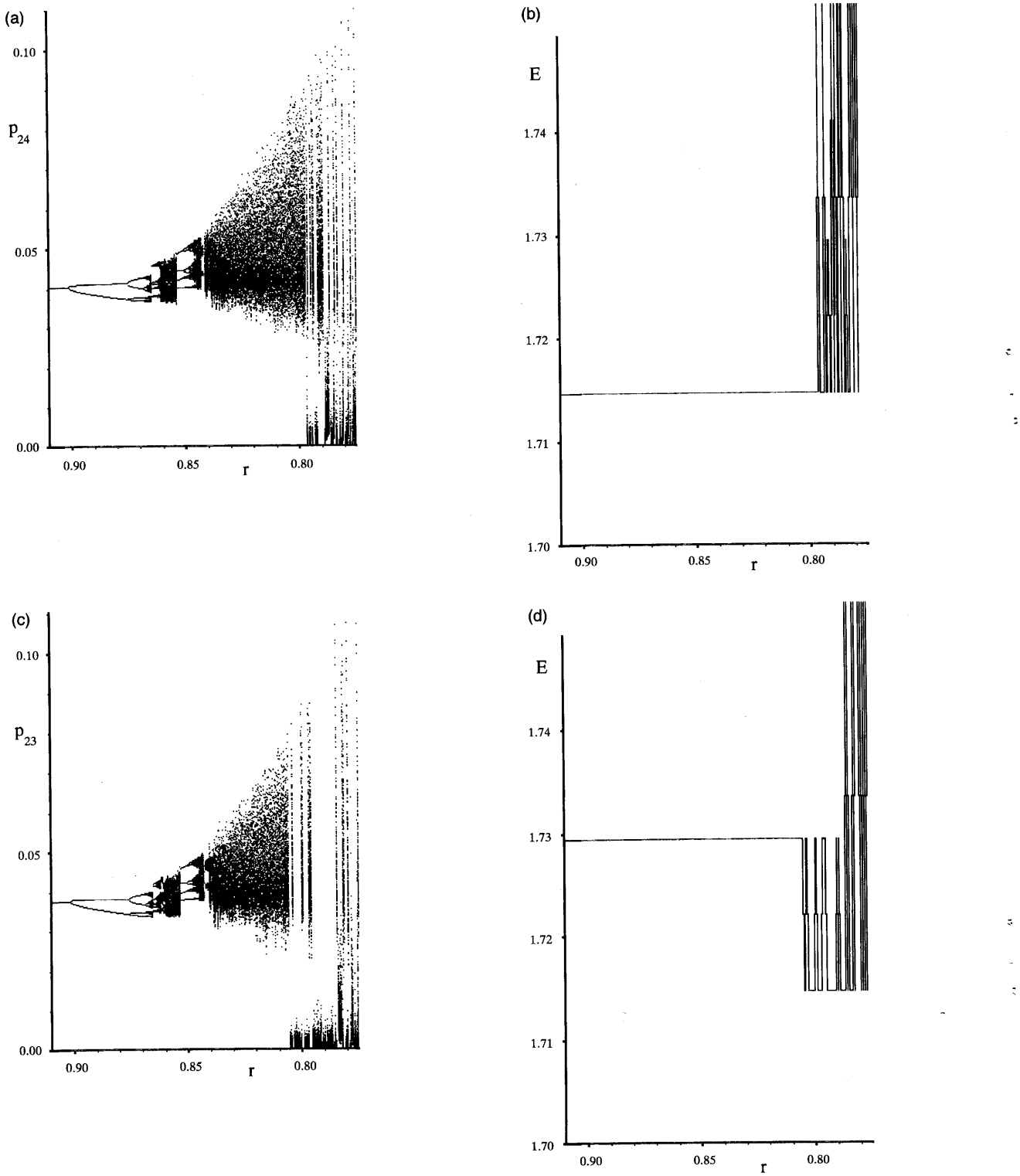

FIGURE 9. A one-parameter bifurcation diagram for the 5-city TSP. The bifurcation parameter value r is decreased from 0.91 to 0.775. (a) A one-parameter bifurcation diagram drawn from a local minimum $q^{(1)}$. (b) The cost function values $E(\bar{J}(O_r^{(1)}))$ for the successively observed attractors $O_r^{(1)}$ in (a). (c) A one-parameter bifurcation diagram drawn from a local minimum $q^{(2)}$. (d) The cost function values $E(\bar{J}(O_r^{(2)}))$ for the successively observed attractors $O_r^{(2)}$ in (c).

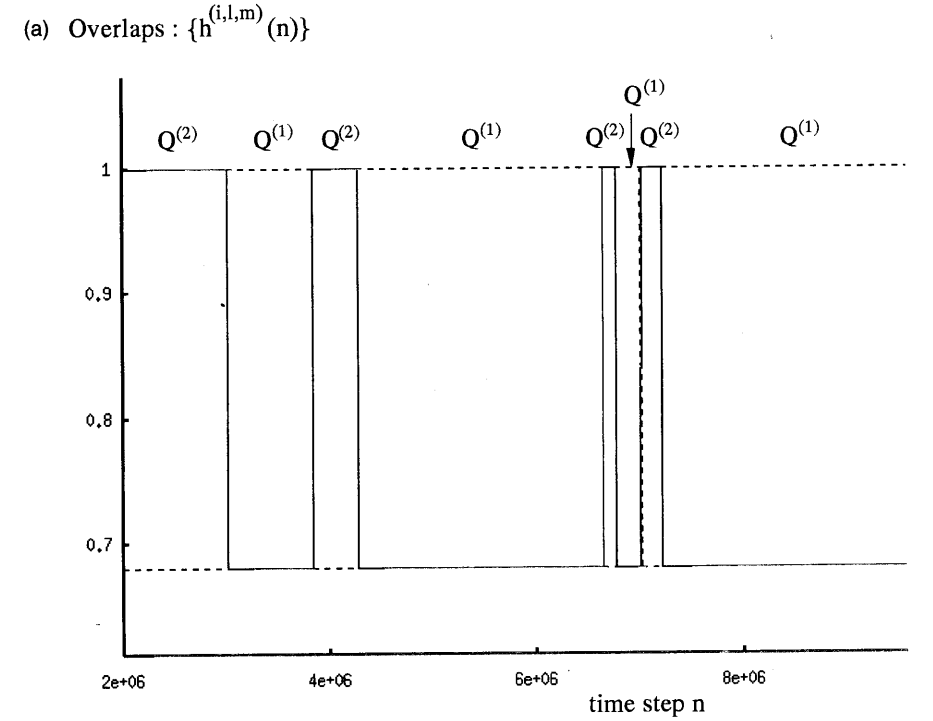

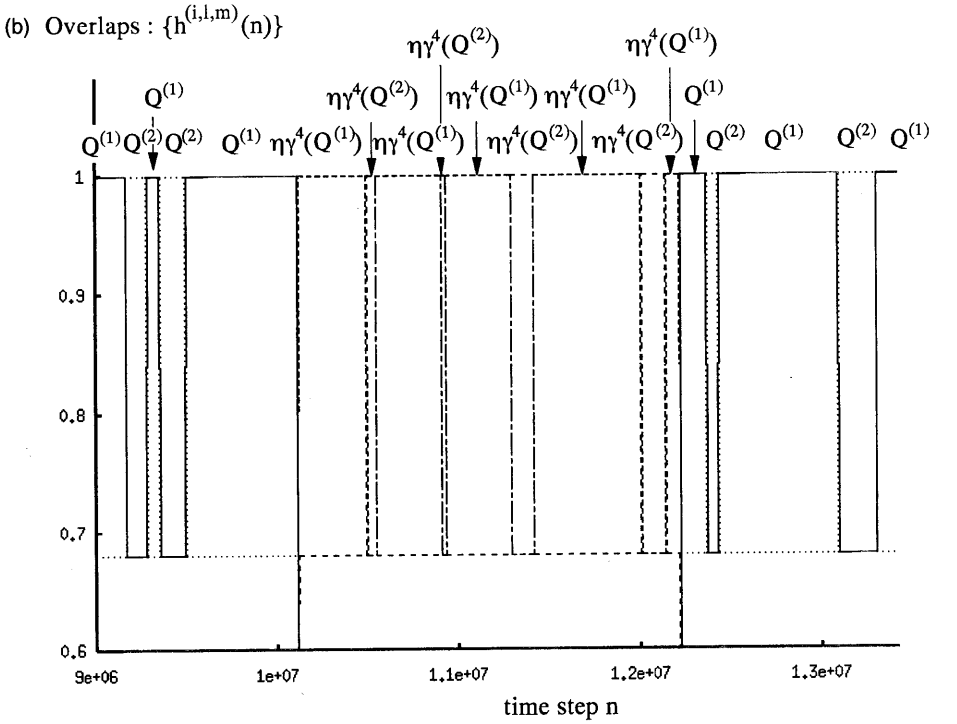

FIGURE 10. Sample sequences $\{\mathcal{J}(n) | \ n = 0,1,\ldots\}$ of the temporal network dynamics with (a) $r = 0.806$ and (b) $r = 0.798$ are shown. The averaging duration of eqn (11) is set to $\omega = 300$. The temporal network state is displayed in terms of a set of overlaps between $\mathcal{J}(n)$ and the previous localized chaotic attractors $\{\eta^l \circ \gamma^m(Q^{(i)}) | \ i = 1,2, \ l = 0,1, \ m = 0,\ldots,4\}$, where the overlap between $\mathcal{J}(n)$ and $\eta^l \circ \gamma^m(Q^{(i)})$ is defined as

$$h^{(i,l,m)}(n) = \frac{1}{N^2} \sum_{j=0}^{N-1} \sum_{k=0}^{N-1} (2\{\eta^l \circ \gamma^m(Q^{(i)})\}_{jk} - 1)(2J_{jk}(n) - 1).$$

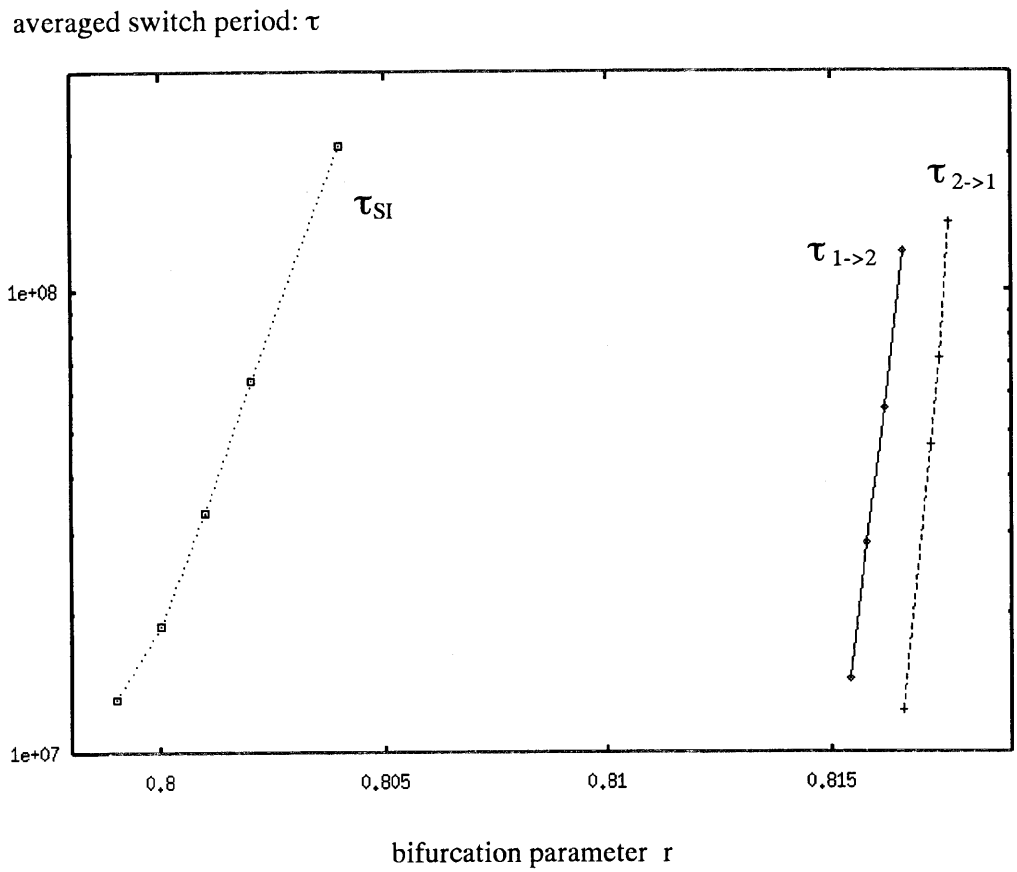

FIGURE 11. The averages of switch durations $\{\tau_{1\to 2}, \tau_{2\to 1}, \tau_{SI}\}$ are drawn with increasing the value of the bifurcation parameter r, where $\tau_{1\to 2}$ denotes the switch duration from $Q^{(1)}$ to $Q^{(2)}$, $\tau_{2\to 1}$ denotes that from $Q^{(2)}$ to $Q^{(1)}$, and τ_{SI} denotes that from $\eta^k\circ\gamma^l(Q^{(l)})$ to $\eta^m\circ\gamma^n(Q^{(l)})$ $((k,l) \neq (m,n))$. With a decrease in the bifurcation parameter, first, switch from $Q^{(2)}$ to $Q^{(1)}$ is observed at $r \cong 0.8176$. Then switch from $Q^{(1)}$ to $Q^{(2)}$ is recognized at $r \cong 0.8166$. Finally, switches among the conjugate attractors $\{\eta^l\circ\gamma^m(Q^{(l)}) \mid l=1,2, l=0,1, m=0,\ldots,4\}$ are observed at $r \cong 0.804$.

network by a carpet-bombing algorithm. For 100,000 samples of random initial conditions which are uniformly distributed over $p(0) \in [0,1]^{N\times N}$, two sets of $2N$ conjugate fixed points $\{\eta^l\circ\gamma^m(q^{(1)}) | l=0,1, m=0,\ldots,N-1\}$ and $\{\eta^l\circ\gamma^m(q^{(2)}) | l=0,1, m=0,\ldots,N-1\}$ are found (see Table 1). Whereas $q^{(1)}$ is coded as the optimum solution $Q^{(1)}$, $q^{(2)}$ is coded as the second-optimum solution $Q^{(2)}$ (see Figure 8).

By decreasing the value of the bifurcation parameter r from 0.91 to 0.775, two bifurcation diagrams are drawn respectively from $q^{(1)}$ and $q^{(2)}$ by observing a single neuron state (see Figure 9(a) and (c)).

In Figure 9(a)–(d), essentially similar bifurcation phenomena to the 10-city instance are observed. Namely, in the first stage of the bifurcation diagram, each local minimum $q^{(i)}$ $(i=1,2)$ undergoes a cascade of period-doubling bifurcations leading to a chaotic attractor. With a further decrease in the bifurcation parameter, each chaotic attractor increases in size. Whereas the repeated occurrence of saddle-node bifurcations gives rise to pairs of stable and unstable periodic solutions generating periodic windows in the bifurcation diagram, the stable periodic attractors also bifurcate into chaotic attractors which soon merge with the original chaotic attractor.

Let us denote the successively observed attractors in each bifurcation diagram as $O_r^{(i)}$ $(i=1,2)$. Their bifurcation phenomena are peculiar at the following points:

1. In each bifurcation diagram, $O_r^{(i)}$ $(i=1,2)$ are continually coded as $Q^{(i)}$ (see Figure 9(b) and (d)).
2. The basins of the two sets of conjugate attractors $\{\eta^l\circ\gamma^m(O_r^{(i)}) \mid i=1,2, \quad l=0,1, \quad m=0,\ldots,N-1\}$ almost always occupy the entire state space (see Table 1).In other words, bifurcation phenomena which give birth to attractors corresponding to TSP solutions other than $Q^{(1)}$ and $Q^{(2)}$ are rarely observed.

As the bifurcation parameter is further decreased, the chaotic attractors $O_r^{(i)}$ $(i=1,2)$ enlarge their sizes. At the parameter value of $r \cong 0.805$, first, $O_r^{(2)}$ disappears from the bifurcation diagram via a boundary crisis to $O_r^{(1)}$. Then $O_r^{(1)}$ collides with the ruin of the previous chaotic attractor $O_r^{(2)}$ via an interior crisis. The merger of $O_r^{(1)}$ and $O_r^{(2)}$ gives rise to a single attractor $O_r^{(1,2)}$ which exhibits intermittent switching among $Q^{(1)}$ and $Q^{(2)}$ (see Figure 10(a)). Finally, for the parameter region of $r < 0.805$, the

conjugate attractors $\{\eta^l \circ \gamma^m(O_r^{(1,2)}) | l = 0,1, m = 0,\ldots, N-1\}$ merge into a single attractor via symmetry-increasing crises. The intermittent switches, or 'chaotic search', for all the previous localized chaotic attractors $\{\eta^l \circ \gamma^m(Q^{(i)}) | i = 1,2, l = 0,1, m = 0,\ldots,N-1\}$ are observed here (see Figure 10(b)). The detailed merging processes are also read from Figure 11, which shows the average of switch duration $\{\tau_{1\to 2}, \tau_{2\to 1}, \tau_{SI}\}$ drawn with increasing the value of the bifurcation parameter r, where $\tau_{1\to 2}$ denotes a switch duration from $Q^{(1)}$ to $Q^{(2)}$, $\tau_{2\to 1}$ denotes a switch duration from $Q^{(2)}$ to $Q^{(1)}$, and τ_{SI} denotes a switch duration from $\eta^k \circ \gamma^l(Q^{(i)})$ to $\eta^m \circ \gamma^n(Q^{(j)})$ $((k,l) \neq (m,n))$.

4.2. Efficiency of the Chaotic Search

Let us discuss the efficiency of the chaotic search for the two TSP instances with small numbers of cities studied in Sections 3 and 4. In case of the 10-city instance, intermittent switch occurs only among a set of equivalent TSP solutions and hence efficiency of the 'chaotic search' for a better solution can not be discussed. For the 5-city instance, chaotic search occurs among the optimum solution $Q^{(1)}$ and the second-optimum solution $Q^{(2)}$. In this case, efficiency of the chaotic search can be discussed in terms of a transition probability between $Q^{(1)}$ and $Q^{(2)}$. The transition probability $T(Q^{(i)} \to Q^{(j)})$ (Kaneko, 1989) represents a probability of transition from $Q^{(i)}$ to $Q^{(j)}$ when the system is trapped in solution $Q^{(i)}$. If the transition probability from $Q^{(2)}$ to $Q^{(1)}$ is higher than that from $Q^{(1)}$ to $Q^{(2)}$, then transitions to optimum solution $Q^{(1)}$ occur more frequently than ones to second-optimum solution $Q^{(1)}$ and hence the dynamics can be considered to be efficient to search for the optimum solution. For $r = 0.80$, the ratio of the transition probabilities $T(Q^{(2)} \to Q^{(1)})$ and $T(Q^{(1)} \to Q^{(2)})$ is calculated as $T(Q^{(2)} \to Q^{(1)})/T(Q^{(1)} \to Q^{(2)}) = 3.31$, which indicates the higher transition probability to the optimum solution $Q^{(1)}$. Therefore we have confirmed efficiency of the chaotic search for the optimum solution in the 5-city instance, although the number of cities is extremely small.

5. CONCLUSIONS AND DISCUSSIONS

5.1. Bifurcation Scenario

On the basis of the several numerical studies, a simple bifurcation scenario is obtained for chaotic neural networks applied to solve TSPs.

First, a one-parameter family of dynamical systems leading the continuous-time Hopfield–Tank neural network to the chaotic neural network is formulated. With a decrease in the bifurcation parameter, local minimum solutions of the Hopfield–Tank neural network undergo period-doubling bifurcation routes leading to chaotic attractors. The chaotic attractors are locally distributed in the state space. As the bifurcation parameter is further decreased, the localized chaotic attractors increase in size and eventually merge into a single global attractor via crises. The merging process gives rise to intermittent switching among the previous localized chaotic attractors. Since the previous localized chaotic attractors are interpreted as possible TSP solutions by introducing a simple coding rule, our bifurcation studies find that the crisis-induced intermittent switches underly the 'chaotic search' for TSP solutions.

We remark that the present bifurcation scenario is obtained only from two instances of small-scale TSP and may not necessarily provide a general bifurcation theory of the chaotic neural networks for the optimization problem. We believe, however, that our bifurcation scenario is still valid for describing the essential features of the chaotic neuro-dynamics which may efficiently work for a wide class of TSPs, since we have confirmed essentially similar bifurcation phenomena in several other instances of TSP.

5.2. Efficiency of the Chaotic Search

On the basis of our bifurcation scenario, let us discuss the optimization capability of the 'chaotic search.' The observed bifurcation phenomena are peculiar in the sense that they rarely give birth to attractors corresponding to TSP solutions except those observed in the local minimum solutions of the underlying Hopfield–Tank neural network. It is most probable that the previous localized chaotic attractors in the 'chaotic search' region are born from period-doubling bifurcations of the local minimum solutions of the Hopfield–Tank neural network and hence they have almost one-to-one correspondence with the local minima. This bifurcation property can be also observed in other instances including higher-dimensional TSPs, although theoretical understanding of this property is an important open question. In the sense that the chaotic dynamics seeks for a better TSP solution among local minimum solutions of the Hopfield–Tank neural network without being trapped in one solution, our bifurcation scenario implies the 'chaotic search' capability which overcomes the weakness of the Hopfield–Tank search.

Our bifurcation studies also imply that the efficiency of the 'chaotic search' strongly depends upon the complex linkage structure of a variety of previous localized chaotic attractors. A large number of dynamical paths leading to a global minimum may produce efficient search for the global minimum, whereas a large number of paths leading to local minima may provide poor results. From this viewpoint, we have studied the 'chaotic search' capability for optimum solution by calculating the transition probabilities among the switching solutions. For the 10-city instance, 'chaotic search' occurs only among a set of equivalent global minimum solutions and hence efficiency of the chaotic switch from local minima to global minimum can not be discussed.

For the 5-city instance, chaotic search occurs among the optimum solution and the second-optimum solution. The transition probability analysis clarified that the chaotic switch to the optimum solution occurs more frequently than that to the second-optimum solution. We therefore confirmed the efficiency of the chaotic search for global minimum solution in this toy problem with 5 cities.

We remark that the present study on the efficiency of the 'chaotic search' provides only preliminary results because our experiments deal with only two small-scale instances of TSP. It is an important future problem to examine the efficiency of the chaotic search for a variety of TSP instances including large-scale problems with further statistical studies based on the calculation of the transition probabilities or other statistical quantities.

It is also necessary to compare the chaotic search algorithm with conventional optimization algorithms such as heuristic algorithms (e.g., Lawler et al., 1985), genetic algorithms (e.g., Goldberg, 1989), and so forth and clarify disadvantages as well as advantages of the chaotic search method. We also remark that our bifurcation analysis provides an insight on the efficiency of the chaotic annealing algorithm (Chen & Aihara, 1995), since the annealing procedure is primarily dependent upon the global bifurcation structure of the chaotic neural network. In the light of the annealing schedule, we can show that an 'infinitely slow annealing' algorithm does not necessarily provide an optimum result and an 'adaptive chaotic annealing' algorithm (Tokuda et al., 1996) works rather fast and efficiently. The detailed result will be reported elsewhere.

5.3. Parameter Tuning

Another problem to be settled for practical application of the present method is the difficulty of choosing good parameter values for $(A, B, \alpha, \omega, r)$ that give rise to efficient 'chaotic search'. In this paper, we have adopted the parameter values of Nozawa (1992) for the 10-city TSP and slightly adjusted the parameter values for the 5-city TSP. Whereas there is no systematic way for determining good parameter values for (A, B, α, ω), the present bifurcation analysis at least provides a hint for tuning the bifurcation parameter value r. Namely, by following the bifurcation procedure of one of the local minima of the Hopfield–Tank neural network, one may find the bifurcation parameter region where the chaotic attractors merge with others via a series of crises and an efficient 'chaotic search' takes place. This reduces the amount of labor for adjusting the bifurcation parameter value r by trial and error methods.

5.4. Chaotic Neural Network as a Coupled Map

Finally, it is also an interesting problem to consider the present chaotic neuro-dynamics from the view point of coupled map studies (Kaneko, 1989, 1990, 1991). As is mentioned in (Kaneko, 1990, 1991; Tsuda, 1991a; Nozawa, 1992), a class of neural network models can be considered as a globally coupled map (Kaneko, 1990, 1991) and the present model can be considered as a globally coupled map with non-uniform couplings, although modeling of chaotic neural networks has its own research history (Aihara & Matsumoto, 1986; Aihara, Kotani, & Matsumoto, 1989; Aihara, 1990). The main difference of the dynamical structure of the present non-uniformly coupled map and the uniformly coupled maps (Kaneko, 1990, 1991) is the degrees of the system symmetry. Compared to the uniform model which has full permutation group S_N as the symmetry (Kaneko, 1990, 1991), the present model has a much lower degree of symmetry due to the non-uniform couplings. As is presented in the studies of the uniformly coupled map models (Kaneko, 1990, 1991), higher symmetry in the dynamical system produces more complex and rich dynamical phenomena induced by the multistability of a large number of conjugate clustering attractors. This might be the reason why the present model as a globally coupled map has a simpler global bifurcation structure rather than the uniformly coupled models. A future problem will be to study how the degree of uniformity in a globally coupled map affects the complexity of the global dynamical structure.

REFERENCES

Adachi, M., & Aihara, K. (1996). Associative dynamics in a chaotic neural network. *Neural Networks*, in press.

Aihara, K. (1990). Chaotic neural network. In H. Kawakami (Ed.), *Bifurcation phenomena in nonlinear systems and theory of dynamical systems* (pp. 143–161). Singapore: World Scientific.

Aihara, K., & Matsumoto, G. (1986). Chaotic oscillations and bifurcations in squid giant axons. In A. V. Holden (Ed.), *Chaos* (pp. 257–269). Manchester: Manchester University Press and Princeton: Princeton University Press.

Aihara, K., Kotani, M., & Matsumoto, G. (1989). Chaos and bifurcations in dynamical systems of nerve membranes. In P.L. Christiansen & R.D. Parmentier (Eds.), *Structure, coherence and chaos in dynamical systems* (pp. 613–617). Manchester: Manchester University Press.

Aihara, K., Takabe, T., & Toyoda, M. (1990). Chiral neural networks. *Physics Letters A, 144,* 333–340.

Aiyer, S.V.B., Niranjan, M., & Frank, F. (1990). A theoretical investigation into the performance of the Hopfield model. *IEEE Transactions on Neural Networks, 1*(2), 204–215.

Chen, L., & Aihara, K. (1995). Chaotic simulated annealing by a neural network model with transient chaos. *Neural Networks, 8*(6), 915–930.

Chossat, P., & Golubitsky, M. (1988a). Iterates of maps with symmetry. *SIAM Journal of Math. Anal., 19,* 1259–1270.

Chossat, P., & Golubitsky, M. (1988b). Symmetry-increasing bifurcations of chaotic attractors. *Physica D, 32,* 423–436.

Garey, M. R. & Johnson, D. S. (1979). *Computers and intractability: A guide to the theory of NP-completeness.* San Francisco: W.H. Freeman.

Goldberg, D.E. (1989). *Genetic algorithms in search, optimization and machine learning.* Reading: Addison Wesley.

Golubitsky, M., Stewart, I.N., & Schaeffer, D.G. (1988). *Singularities*

and groups in bifurcation theory II, Applied Mathematical Science Series (p. 69). Berlin: Springer-Verlag.

Grebogi, C., Ott, E., Romeiras, F., & York, J.A. (1987). Critical exponents for crisis-induced intermittency. *Physical Review A, 36,* 5365–5380.

Grebogi, C., Ott, E., & York, J.A. (1982). Chaotic attractors in crisis. *Physical Review Letters, 48,* 1507–1510.

Hegde, S.U., Sweet, J.L., & Levy, W.B. (1988). Determination of parameters in a Hopfield/Tank computational network. *Proceedings of IEEE International Conference on Neural Networks, San Diego,* Vol. II (pp. 291–298). New York: IEEE.

Hopfield, J.J., & Tank, D.W. (1985). Neural computation of decisions in optimization problems. *Biological Cybernetics, 52,* 141–152.

Ikeda, K., & Matsumoto, K. (1987). High-dimensional chaotic behavior in systems with time-delayed feedback. *Physica D, 29,* 223–235.

Ikeda, K., Otsuka, K., & Matsumoto, K. (1989). Maxwell–Bloch turbulence. *Progress of Theoretical Physics, Supplement, 99,* 295–324.

Kaneko, K. (1989). Pattern dynamics in spatiotemporal chaos—Pattern selection, diffusion of defect and pattern competition intermittency. *Physica D, 34,* 1–41.

Kaneko, K. (1990). Clustering, coding, switching, hierarchical ordering, and control in a network of chaotic elements. *Physica D, 41,* 137–172.

Kaneko, K. (1991). Globally coupled circle maps. *Physica D, 54,* 5–19.

Kaplan, J.L., & York, J.A. (1987). Chaotic behaviour of multi-dimensional difference equations in functional differential equations and approximations of fixed points. In *Lecture notes in mathematics,* Vol. 730 (pp. 204–227). Berlin: Springer-Verlag.

Kirkpatrick, S., Gelatt Jr, C.D., & Vecchi, M.P. (1983). Optimization by simulated annealing. *Science, 220,* 671–680.

Lawler, E.L., Lenstra, J.K., Rinnooy Kan, A.H.G., & Shmoys, D.B. (1985). *The traveling salesman problem.* New York: Wiley.

Nagashima, T., Shiroki, Y., & Tokuda, I. (1996). A scenario for the onset of dynamical associative memory in chaotic neural network. *Proceedings of The 4th International Conference on Soft Computing, Iizula,* Vol. 2 (pp. 692–695). Singapore: World Scientific.

Nozawa, H. (1992). A neural network model as a globally coupled map and applications based on chaos. *Chaos, 2*(3), 377–386.

Nozawa, H. (1994). Solution of the optimization problem using the neural network model as a globally coupled map. In M. Yamaguti (Ed.), *Towards the harnessing of chaos* (pp. 99–114). Amsterdam: Elsevier.

Ohta, M., Anzai, Y., Yoneda, S., & Ogihara, A. (1993). A theoretical analysis of neural networks with nonzero diagonal elements. *IEICE Transactions on Fundamentals, E76-A,* 284–291.

Pineda, F.J. (1988). Dynamics and architecture for neural computation. *Journal of Complexity, 4,* 216–245.

Reeves, C.R. (1993). *Modern heuristic techniques for combinatorial problems.* Oxford: Blackwell.

Skarda, C.A., & Freeman, W.J. (1987). How brains make chaos in order to make sense of the world. *Behavioral and Brain Sciences, 10,* 161–195.

Tokuda, I., Aihara, K., & Nagashima, T. (1996). Adaptive annealing for chaotic optimization. *Proceedings of The Symposium on Nonlinear Theory and its Applications, Katsurahama* (pp. 281–284). Tokyo: IEICE.

Tsuda, I. (1991a). Chaotic itinerancy as a dynamical basis of Hermeneutics in brain and mind. *World Futures, 32,* 167–184.

Tsuda, I. (1991b). Chaotic neural networks and thesaurus. In A.V. Holden & V.I. Kryukov (Eds.), *Neurocomputers and attention I* (pp. 405–424). Manchester University Press: Manchester.

Tsuda, I. (1992). Dynamics link of memory—Chaotic memory map in nonequilibrium neural networks. *Neural Networks, 5,* 313–326.

Tsuda, I., Koerner, E., & Shimizu, H. (1987). Memory dynamics in asynchronous neural networks. *Progress of Theoretical Physics, 78,* 51–71.

Willson, G.V., & Pawley, G.S. (1988). On the stability of the travelling salesman problem algorithm of Hopfield and Tank. *Biological Cybernetics, 58,* 63–70.

Yamada, T., & Aihara, K. (1994). Dynamical neural networks and the traveling salesman problem. In M. Yamaguti (Ed.), *Towards the harnessing of chaos* (pp. 423–426). Amsterdam: Elsevier.

Yamada, T., Aihara, K., & Kotani, M. (1993). Chaotic neural networks and the traveling salesman problem. *Proceedings of the International Joint Conference on Neural Networks, Nagoya,* Vol. 2 (pp. 1549–1552). New York: IEEEE.

Yao, Y., & Freeman, W.J. (1987). Models of biological pattern recognition with spatially chaotic dynamics. *Neural Networks, 3,* 153–170.

APPENDIX A: SYMMETRY IN DYNAMICAL SYSTEMS

In this Appendix, we show (1): $f\circ\gamma = \gamma\circ f$ and (2): $f\circ\eta = \eta\circ f$. (1) and (2) immediately lead to $f\circ(\eta^l\circ\gamma^m) = (\eta^l\circ\gamma^m)\circ f$ for $l = 0,1$ and $m = 0,\ldots, N-1$.

(1) For any $p \in R^{N\times N}$, $f\circ\gamma(p) = \gamma\circ f(p)$ because

$$\{f\circ\gamma(p)\}_{ik} = r\,p_{i\,k+1} + (1-r)\sigma\left(\sum_{j=0}^{N-1}\sum_{l=0}^{N-1} T_{ik,\,jl}p_{j\,l+1} + I\right) \tag{A.1}$$

$$= r\,p_{i\,k+1} + (1-r)\sigma\left(\sum_{j=0}^{N-1}\sum_{l'=0}^{N-1} T_{ik,\,jl'-1}p_{jl'^{prime}} + I\right) \tag{A.2}$$

$$= r\,p_{i\,k+1} + (1-r)\sigma\left(\sum_{j=0}^{N-1}\sum_{l'=0}^{N-1} T_{i\,k+1,\,jl'}p_{jl'} + I\right) \tag{A.3}$$

$$= \{f(p)\}_{ik+1} = \{\gamma\circ f(p)\}_{ik} \tag{A.4}$$

for $0 \le i,k \le N-1$. The indices in $\{I_{ik}\}$ are dropped since the set of the parameters $\{I_{ik}\}$ takes a same value by eqn (8). From eqns (A.2) to (A.3), we have used $T_{ik,\,jl-1} = T_{ik+1,\,jl}$, which is the property of the synaptic connections defined by eqns (6)–(7).

(2) For any $p \in R^{N\times N}$, $f\circ\eta = \eta\circ f$ because

$$\{f\circ\eta(p)\}_{ik} = r\,p_{i\,N-k} + (1-r)\sigma\left(\sum_{j=0}^{N-1}\sum_{l=0}^{N-1} T_{ik,\,jl}p_{jN-l} + I\right) \tag{A.5}$$

$$= r\,p_{i\,N-k} + (1-r)\sigma\left(\sum_{j=0}^{N-1}\sum_{l'=0}^{N-1} T_{ik,\,jN-l'}p_{jl'} + I\right) \tag{A.6}$$

$$= r\,p_{i\,N-k} + (1-r)\sigma\left(\sum_{j=0}^{N-1}\sum_{l'=0}^{N-1} T_{i\,N-k,\,jl'}p_{jl'} + I\right) \tag{A.7}$$

$$= \{f(p)\}_{i\,N-k} = \{\eta\circ f(p)\}_{ik} \tag{A.8}$$

for $0 \le i,k \le N-1$. From eqn (A.6) to eqn (A.7), we have used $T_{ik,jN-l}\} = T_{iN-k,\,jl}$, which is the property of the synaptic connections defined by eqns (6)–(7).

APPENDIX B: CONJUGATE ATTRACTORS WITH AN EQUIVALENT TSP SOLUTION

This Appendix shows how the system symmetry gives rise to $2N$ conjugate attractors representing an equivalent TSP solution.

Suppose there exists an asymmetric attractor $O = \{p(n)|n = 0,1,\ldots\}$ which is coded as a feasible TSP solution $\bar{J}(\bar{\rho})$, where $\bar{\rho} = \lim_{T\to\infty}(1/T)\sum_{n=0}^{T-1}p(n)$ represents a long-term average firing rate of O.

For all $l = 0,1$ and $m = 0,\ldots,N-1$, a long-term average firing rate of a conjugate attractor $\eta^l\circ\gamma^m(O)$ ($= \{\eta^l\circ\gamma^m((p(n))|\ n = 0,1,\ldots\})$ can be written as $\eta^l\circ\gamma^m(\bar{\rho})$ because a linear mapping $\eta^l\circ\gamma^m$ transforms $\bar{\rho}$ into $\eta^l\circ\gamma^m(\bar{\rho}) = \lim_{T\to\infty}(1/T)\sum_{n=0}^{T-1}\eta^l\circ\gamma^m(p(n))$. Since $\bar{J}(\eta^l\circ\gamma^m(\bar{\rho})) =$

$\eta^l \circ \gamma^m(\bar{J}(\bar{\rho}))$, the $2N$ conjugate asymmetric attractors $\{\eta^l \circ \gamma^m(O) | l = 0,1, m = 0,\ldots,N-1\}$ are coded respectively as $\{\eta^l \circ \gamma^m(\bar{J}(\bar{\rho})) | l = 0,1, m = 0,\ldots,N-1\}$.

It is well known that the $2N$ codes $\{\eta^l \circ \gamma^m(\bar{J}(\bar{\rho})) | l = 0,1, m = 0,\ldots, N-1\}$ represent an equivalent TSP solution (Hopfield & Tank, 1985). This is because the transformations γ and η do not change the basic tour configuration. Namely, γ only shifts a choice of an initial city in a visiting order of the cities and η changes a choice of a visiting direction of the cities. Hence, the $2N$ conjugate attractors $\{\eta^l \circ \gamma^m(O) | l = 0,1, m = 0,\ldots,N-1\}$ are coded into an equivalent TSP solution..